frontiers | Frontiers in Aging Neuroscience

ORIGINAL RESEARCH
published: 06 July 2022
doi: 10.3389/fnagi.2022.946297

Aβ/Amyloid Precursor Protein-Induced Hyperexcitability and Dysregulation of Homeostatic Synaptic Plasticity in Neuron Models of Alzheimer's Disease

Isak Martinsson[1,2], Luis Quintino[3], Megg G. Garcia[1,2], Sabine C. Konings[1], Laura Torres-Garcia[1,4], Alexander Svanbergsson[4], Oliver Stange[1], Rebecca England[1], Tomas Deierborg[2], Jia-Yi Li[4], Cecilia Lundberg[3] and Gunnar K. Gouras[1]**

[1] Experimental Dementia Research Unit, Department of Experimental Medical Science, Lund University, Lund, Sweden, [2] Experimental Neuroinflammation Unit, Department of Experimental Medical Science, Lund University, Lund, Sweden, [3] CNS Gene Therapy, Department of Experimental Medical Science, Lund University, Lund, Sweden, [4] Neural Plasticity and Repair, Department of Experimental Medical Science, Lund University, Lund, Sweden

Alzheimer's disease (AD) is increasingly seen as a disease of synapses and diverse evidence has implicated the amyloid-β peptide (Aβ) in synapse damage. The molecular and cellular mechanism(s) by which Aβ and/or its precursor protein, the amyloid precursor protein (APP) can affect synapses remains unclear. Interestingly, early hyperexcitability has been described in human AD and mouse models of AD, which precedes later hypoactivity. Here we show that neurons in culture with either elevated levels of Aβ or with human APP mutated to prevent Aβ generation can both induce hyperactivity as detected by elevated calcium transient frequency and amplitude. Since homeostatic synaptic plasticity (HSP) mechanisms normally maintain a setpoint of activity, we examined whether HSP was altered in AD transgenic neurons. Using methods known to induce HSP, we demonstrate that APP protein levels are regulated by chronic modulation of activity and that AD transgenic neurons have an impaired adaptation of calcium transients to global changes in activity. Further, AD transgenic compared to WT neurons failed to adjust the length of their axon initial segments (AIS), an adaptation known to alter excitability. Thus, we show that both APP and Aβ influence neuronal activity and that mechanisms of HSP are disrupted in primary neuron models of AD.

Keywords: amyloid, APP – amyloid precursor protein, synapse, calcium imaging, homeostatic synaptic plasticity (HSP), neuron

OPEN ACCESS

Edited by:
Jorge Busciglio, University of California, Irvine, United States

Reviewed by:
Agenor Limon, University of Texas Medical Branch at Galveston, United States
Rakez Kayed, University of Texas Medical Branch at Galveston, United States
Alfredo Lorenzo, Instituto Ferreyra – INIMEC-CONICET-UNC, Argentina

****Correspondence:***
Isak Martinsson
isak.martinsson@med.lu.se
Gunnar K. Gouras
gunnar.gouras@med.lu.se

Specialty section:
This article was submitted to Cellular and Molecular Mechanisms of Brain-aging, a section of the journal Frontiers in Aging Neuroscience

Received: *17 May 2022*
Accepted: *16 June 2022*
Published: *06 July 2022*

Citation:
Martinsson I, Quintino L, Garcia MG, Konings SC, Torres-Garcia L, Svanbergsson A, Stange O, England R, Deierborg T, Li J-Y, Lundberg C and Gouras GK (2022) Aβ/Amyloid Precursor Protein-Induced Hyperexcitability and Dysregulation of Homeostatic Synaptic Plasticity in Neuron Models of Alzheimer's Disease. Front. Aging Neurosci. 14:946297. doi: 10.3389/fnagi.2022.946297

INTRODUCTION

Alzheimer's disease (AD) is the leading cause of dementia and the most common neurodegenerative disease. AD is characterized by the progressive, age-related accumulation and aggregation of disease-associated proteins, in particular amyloid-β (Aβ), which is cleaved from the amyloid precursor protein (APP). Multiple lines of genetic, clinical and biological evidence support the

involvement of Aβ in driving the loss of synapses and neurons that characterize the disease. However, preceding the massive neurodegeneration, AD features aberrant regional neuronal activity in the form of both hyper- and hypo-excitability, and evidence supports that the occurrence of network hyper-excitability early in the disease process is tied to elevated Aβ levels (Vossel et al., 2013; Zott et al., 2019). However, the precise mechanisms underlying this early Aβ-induced hyper-excitability remain unclear. In addition, the normal roles of Aβ/APP in brain physiology and their roles in pathophysiology during AD remain incompletely understood. Numerous lines of evidence indicate that synapses are sites of early pathogenesis in AD. APP mRNA is locally translated at post-synapses (Westmark and Malter, 2007) and APP protein is transported by fast axonal transport down axons (Koo et al., 1990), and the machinery to process APP to Aβ is localized to both pre- and post-synaptic sites. The presynaptic site is generally considered to process more APP to Aβ (Sadleir et al., 2016), although the role of neuron subtypes and anatomy in the subcellular location and generation of Aβ in brain remain poorly understood. The CA3 mossy fiber axonal terminals in the hippocampus, for example, are a site of high BACE1 levels and therefore could lead to high APP processing at presynapses (Sadleir et al., 2016). Numerous studies have reported detrimental electrophysiological, biological and behavioral effects of exogenously added Aβ on primary neurons, brain slices or murine brains *in vivo* (Abramov et al., 2009; Minkeviciene et al., 2009; Faucher et al., 2016). Emerging work indicates a complex interrelationship between intra- and extra-neuronal pools of Aβ, with the intraneuronal pool accumulating early on, prior to plaques (Roos et al., 2021). Aβ was shown to accumulate aberrantly in endosomes near synapses (Takahashi et al., 2002), where it can impair important endocytic pathways at synapses (Almeida et al., 2006). Normal synaptic function relies on regulated recycling, retrograde transport, secretion and degradation *via* endosomes that can be impaired by such aberrant protein aggregation (Perdigão et al., 2020). It is of considerable importance to parse out the earliest molecular steps in this synaptic dysfunction with AD. Primary cultures of neurons from AD transgenic mice have replicated *in vivo* phenotypes seen in AD, including increased endosome size (Willén et al., 2017) and loss of spines (Kashyap et al., 2019), and have shown Aβ-dependent reductions in important synaptic proteins, such as glutamate receptors, PSD-95 and synaptophysin (Almeida et al., 2005). Untangling the relative roles of Aβ and APP in AD also remains incomplete.

The coordinated firing of neurons across networks is considered to be crucial for cognitive function. To maintain their proper function and levels of activity, neurons employ homeostatic synaptic plasticity (HSP) and homeostatic intrinsic plasticity (HIP), which are means by which neurons can tune their activity to the global tonus of activity. Homeostatic scaling is an example of one such a tuning mechanism (Turrigiano et al., 1998), and other mechanisms of regulation are being investigated. These modulatory processes enable neuronal communication to be maintained within an appropriate window, allowing meaningful information transfer (Turrigiano, 2012). Recently, both APP and Aβ were implicated in the regulation of HSP (Gilbert et al., 2016; Galanis et al., 2021), indicating that these proteins play important roles beyond AD pathophysiology. Further, prior *in vivo* work in AD transgenic mice has suggested that HSP mechanisms might be impaired, since chronic hypo- or hyper-activity *via* either long term sleep deprivation or induction, or unilateral whisker removal, conditions in which HSP should be engaged, negatively impacted AD transgenic compared to wild-type (WT) mice (Kang et al., 2009; Tampellini et al., 2010). Recently, firing rate homeostasis was shown to be defective in APP/PS1 mice during sleep (Zarhin et al., 2022).

In this study, we set out to further elucidate the effects of APP and Aβ on calcium homeostasis in cultured primary neurons, a model system that allows for the exploration of underlying molecular and cellular biology more easily than *in vivo* in brain. To that end, we utilized primary neuronal cultures from APP/PS1 AD mutant transgenic mice and their WT counterparts and live-cell calcium imaging as a proxy for activity analyses of neuronal networks. We demonstrate that a general increase in transient calcium frequencies occurs both in the context of elevated APP or Aβ. Furthermore, we show that specifically CaMKII-positive excitatory neurons from AD transgenic mice exhibit higher amplitude calcium transients. Finally, we demonstrate the impaired ability of AD transgenic compared to WT neurons to properly initiate homeostatic plasticity mechanisms to adapt to global activity changes.

MATERIALS AND METHODS

Antibodies

The antibodies employed in this study were the following: mouse anti-beta-actin (Sigma-Aldrich, Sweden), rabbit anti-OC against high molecular weight Aβ (Merck Millipore, Sweden), mouse anti-6E10 for human Aβ/APP (BioLegend, Sweden), APPY188 rabbit anti C-terminal APP (Abcam, Sweden), rabbit anti-somatostatin (Abbexa, United Kingdom), mouse anti-GAD67 (Merck Millipore, Sweden), mouse anti-CaMKII (Merck Millipore, Sweden), mouse anti-ankyrin-G (Thermo Scientific, Sweden), guinea pig anti-Vglut1 (Synaptic Systems, Germany), rabbit anti-VGAT (Synaptic systems, Germany), rabbit anti-Gephyrin (Synaptic Systems, Germany), and chicken anti-MAP2 (Abcam, United Kingdom).

Neuronal Cell Culture

Primary neurons were cultured from the cortices and hippocampi of APP/PS1 AD transgenic mouse (APPswe, PSEN1dE9)85Dbo/Mmjax; Jackson Labs, Bar Harbor, ME, United States) and APP KO (Jackson labs, Bar Harbor, ME, United States, JAX 004133) mouse embryos at embryonic days 15–17 (E15-17). Neurons were cultured as previously described (Willén et al., 2017). Briefly, pregnant mice were anesthetized using isoflurane (MSD Animal Health, Stockholm, Sweden) and sacrificed. Embryos were quickly removed, and biopsies were taken for genotyping. Brains were dissected under constant cooling with chilled (∼4°C) Hanks balanced salt solution (HBSS; Thermo Scientific, Sweden) supplemented with 0.45% glucose (Thermo Scientific, Sweden). Cortices and hippocampi were

retrieved and incubated in 0.25% trypsin (Thermo Scientific, Sweden), followed by 2 washes with HBSS. Brain tissue was then triturated in 10% fetal bovine serum (FBS) supplemented Dulbecco's modified Eagle medium (DMEM; Thermo Scientific, Sweden) with 1% penicillin-streptomycin (Thermo Scientific, Sweden) using glass pipettes until neurons were dissociated. Neurons were plated onto 8 well- plates (for calcium imaging; Ibidi), 6 well plates (for Western blot; Sarstedt, Germany) or glass coverslips in 24 well plates (for immunolabeling; Sarstedt, Germany) coated with Poly-D-lysine (Sigma-Aldrich, Sweden). Neurons were plated with 10% FBS and 1% penicillin-streptomycin in DMEM; following 3–5 h incubation, media was exchanged for complete Neurobasal solution, consisting of Neurobasal medium, B27 supplement, penicillin-streptomycin, and L-glutamine (Thermo Scientific, Sweden). One embryo corresponds to one set of cultures. All animal experiments were performed in accordance with the ethical guidelines and were approved by the Animal Ethical Committee at Lund University ethical permit number 5.8.18-05983/2019.

Genotyping

Genotyping was carried out using the PCRbio Rapid Extract PCR kit (Techtum, Sweden). In brief, biopsies were incubated with 70 μl distilled H_2O, 20 μl 5× PCRbio buffer A (lysis buffer) and 10 μl 10× PCRbio buffer B (protease containing buffer) per vial at 75°C for 5 min, followed by heating to 95°C for 10 min. The vials were placed on ice and allowed to cool before vortexing for 3–4 s and centrifuged at 10,000 rpm for 1 min to pellet the debris. The DNA supernatant was then transferred to a new vial. The DNA supernatant was either used directly or stored at −20°C. For PCR, 1 μl of DNA was incubated with 9.5 μl distilled H_2O, 12.5 μl 2× PCRbio rapid PCR mix (containing Taq polymerase for DNA amplification), 1 μl primer-set F (APP knockout) and 1 μl primer-set G (APP WT; both 10 μM) for 3 min at 95°C. The temperature was decreased to 55°C for 15 s to allow for the annealing of primers. The temperature was then increased to 72°C for 5 min to allow for the extension of DNA. DNA bands were detected using agarose gel electrophoresis.

Viral Vectors

We used lentiviral vectors carrying TdTomato, hAPPwt, or hAPPmv (mutant APP resistant to BACE cleavage) under a CaMKII promoter; the genes were inserted *via* Gene synthesis (Thermo Fischer Scientific, United Kingdom) into a plasmid compatible with Gateway technology to serve as an entry clone. Production and titration were performed as previously described (Quintino et al., 2013). Primary neurons were transduced at 12–13 days *in vitro* (DIV) at a multiplicity of infection (MOI) of 5 and analyzed at 19–21 DIV.

Treatments

Cultured neurons at 19–21 DIV were treated with different compounds before live cell imaging, immunofluorescence or western blot experiments: thiorphan (500 nM, 1 h; Sigma-Aldrich, Sweden), TTX [1 μM, acute (0–1 h) or 48 h], bicuculline [20 μM, acute (0–1 h) or 48 h], picrotoxin (10 μM, 1 h), CNQX (10 μM, 1 h) (Sigma-Aldrich, Sweden), and synthetic Aβ1-42 (Tocris, United Kingdom) and synthetic reverse Aβ42-1 (Tocris, United Kingdom) reconstituted in dimethyl sulfoxide (DMSO) to 250 mM, sonicated 10 min and then centrifuged at 10,000 g for 15 min before adding the supernatant to cell culture media.

Western Blot

Cell lysates were prepared using modified RIPA buffer containing 50 mM Tris-HCl (pH 7.4), 150 mM NaCl, 1 mM EGTA, 1% NP-40, 0.25% sodium deoxycholate with added protease and phosphatase inhibitor cocktail II (Sigma-Aldrich, Sweden). BCA protein assay kit (Thermo Scientific, Sweden) was used to determine protein concentrations. Equal amounts of protein from each sample were loaded into 10–20% Tricine sodium dodecyl sulfate–polyacrylamide gel electrophoresis (SDS-PAGE; Sigma-Aldrich, Sweden), followed by immunoblotting on polyvinylidene difluoride (PVDF) membranes (Sigma-Aldrich, Sweden) and intensity quantification was carried out using Image Lab 5.2.1.

Live-Cell Imaging

Cultured neurons at 19–21 DIV were incubated with 3 μM of the calcium dye Fluo-4 AM (Thermo Scientific, Sweden) in DMSO (Sigma-Aldrich, Sweden) for 30 min before imaging. Cells were imaged under a Nikon Eclipse Ti microscope at 10× with 1.4 NA. Live cell imaging chamber (Okolab, Italy) was kept at 5% CO_2 and 37°C. Cells were imaged every 100 ms for a duration of 2 min with an iXon Ultra CCD camera (ANDOR Technology, United Kingdom). Multiple 2 min timestacks were captured from each experimental group.

Calcium Imaging Analysis

Time-stacks of calcium imaging files were opened in FiJi; individual Regions of interest (ROIs) were drawn around cell bodies and ROIs were determined to be CaMKII+ or CaMKII- based on TdTomato labeling. Fluorescence intensity over time was extracted, processed and normalized in the MatLab script PeakCaller (Artimovich et al., 2017). Spike frequencies and amplitudes were extracted, and raster plots were generated in MatLab. Spike detection threshold was set to 10% above baseline; for calculation of frequency all neurons including silent (<1 Peak per 2 min) were included in analysis. For calculation of amplitude heights and interspike intervals, however; silent neurons were excluded as these would bias the measurement and underestimate the amplitude heights and give misleading values in interspike intervals. Therefore number of neurons differ between frequency measurements and amplitude/interspike interval measurements.

Immunofluorescence

Cultured neurons at 19–21 DIV were fixed in 4% paraformaldehyde (PFA) in PBS with 0.12 M sucrose for 20 min, at room temperature (RT). Cells were then blocked in 0.1% saponin (Sigma-Aldrich, Sweden), 1% bovine serum albumin (BSA; Sigma-Aldrich, Sweden) and 2% normal goat serum (NGS; Thermo Scientific, Sweden) in PBS for 1 h at RT. Cells were incubated in primary antibody (diluted in 2% NGS in PBS) overnight at 4°C. Cells were rinsed in PBS and incubated

with secondary antibodies diluted in 2% NGS in PBS. Cells were rinsed in PBS and counterstained with DAPI diluted at 1:2000 (Sigma-Aldrich, Sweden). Imaging was performed with an inverted Olympus IX70 epifluorescence or an inverted Leica SP8 confocal microscope.

Image Analysis

Neurons were labeled for inhibitory or excitatory pre- and post-synaptic markers; CaMKII and VGLUT1 for excitatory synapses and Gephyrin and VGAT for inhibitory synapses. Images were then processed in the ImageJ plugin: SynaptcountJ. SynaptCountJ is a semi-automated plugin for measuring synapse density (Mata et al., 2017). By colocalization of two different excitatory or inhibitory synaptic markers one can count the number of excitatory and inhibitory synapses per neuron along with other morphological parameters such as dendritic length. For CaMKII cell quantification 19–21 DIV APP/PS1 and WT neuronal cultures were labeled with DAPI, CaMKII, and MAP2. Images were sampled at 20× in an inverted Olympus IX70 epifluorescence microscope and analyzed with the "cell-counter" plugin in ImageJ as percent CaMKII positive out of all MAP2 positive neurons. For analysis of axon initial segment length, ankyrin-G positive axon initial segments were traced and measured in ImageJ by a blinded experimenter.

Experimental Design and Statistical Analysis

All statistical analyses were performed with GraphPad Prism 8.3. Sample size was denoted as n = number of cells analyzed and N = sets of cultures. Data was first tested for normality using D'Agostino-Pearson omnibus K2 normality test to determine the appropriate statistical test. No specific statistical analysis was performed to determine sample size. Mann–Whitney (two groups) or Kruskal–Wallis (3 or more groups) tests were used to compare distribution of data between groups unless otherwise stated. Correction for multiple testing was performed with Dunn's correction unless otherwise stated. Graphs are expressed as mean ± 95% confidence interval (CI) with individual values plotted as dots unless otherwise stated in figure legend. Differences were considered significant at $^{*}p < 0.05$, $^{**}p < 0.01$, $^{***}p < 0.001$; $^{****}p < 0.0001$, n.s., not significant.

RESULTS

Characterization of Corticohippocampal Amyloid Precursor Protein/PS1 Transgenic Cultures

To study AD-related neuronal activity alterations *in vitro*, primary cortico-hippocampal neurons from APP/PS1 AD transgenic mice and their WT littermates were loaded with the calcium indicator Fluo-4 AM and imaged for calcium transients using a live cell imaging microscope. Mixed cortico-hippocampal neurons were used, since AD is characterized by cortical and hippocampal pathology. Live cell calcium imaging is used as a proxy of neuronal activity, although actual neuronal excitation and firing can deviate significantly from calcium levels (Gavello et al., 2018). Representative raster plots and calcium traces demonstrate that neurons from both APP/PS1 transgenic and WT mice were spontaneously active (**Supplementary Figures 1A–D**). APP/PS1 neurons overall had increased frequencies of calcium transients and higher amplitudes of calcium spikes compared to WT neurons (**Figures 1A–D**). Inter-spike intervals were also altered in APP/PS1 neurons, which had shorter inter-spike intervals than WT neurons (**Figure 1E**). Moreover, APP/PS1 cultures had fewer inactive neurons compared to WT cultures (**Figure 1F**), consistent with the other signs of increased excitability.

During early development, GABA can have excitatory effects in culture (Doshina et al., 2017). Normally, GABA signaling in culture shifts to being primarily inhibitory at around 14 days *in vitro* (DIV). However, because APP/PS1 neurons may have altered neuronal development due to constitutively over-expressing mutant APP and presenilin (Handler et al., 2000; Rama et al., 2012), the increased activity seen in 19–21 DIV cultures could, in part, have been due to excitatory GABA signaling. Thus, we tested whether GABA signaling had inhibitory or excitatory effects in our presumably mature 19–21 DIV APP/PS1 neurons by treating them with $GABA_A$ blockers bicuculline and picrotoxin. Blocking GABA signaling in the APP/PS1 cultures led to an increased frequency and synchronicity of firing, indicating that GABA had inhibitory effects in our cultures similar to that of WT cultures (**Figure 1G**). The addition of 1 μm TTX stopped most calcium transients in both WT and APP/PS1 neurons (**Figure 1G**), indicating that the majority of calcium transients that were detected were triggered by sodium channel activity.

Hyperactivity of Excitatory Neurons in Amyloid Precursor Protein/PS1 Cultures

To parse out the contributions of excitatory and inhibitory neurons in driving the hyperactivity in APP/PS1 cultures, we transduced neurons with a vector to induce the expression of TdTomato under a CaMKII promoter (**Figure 2A**), allowing us to distinguish excitatory neurons from putative GABAergic interneurons (**Figure 2B**) in imaged FOVs. Interestingly, we detected increased activity in CaMKII-positive APP/PS1 neurons compared to CaMKII-positive WT neurons. In contrast, activity levels in CaMKII-negative neurons were similar between APP/PS1 and WT cultures (**Figure 2C**). Furthermore, CaMKII-positive neurons had higher amplitude calcium transients compared to CaMKII-negative neurons in APP/PS1 but not WT cultures (**Figure 2D**).

We next sought to investigate whether an imbalance in the proportion of excitatory to inhibitory neurons and synapses could underlie the increased levels of activity in APP/PS1 neurons. To do this, we evaluated the relative levels of select proteins known to be localized in either excitatory or inhibitory neurons. Immunoblotting against CaMKII and GAD67, markers expressed by nearly all excitatory and inhibitory neurons, respectively, showed no differences in the levels of CaMKII and GAD67 between APP/PS1 and WT neurons (**Figures 3A–C**).

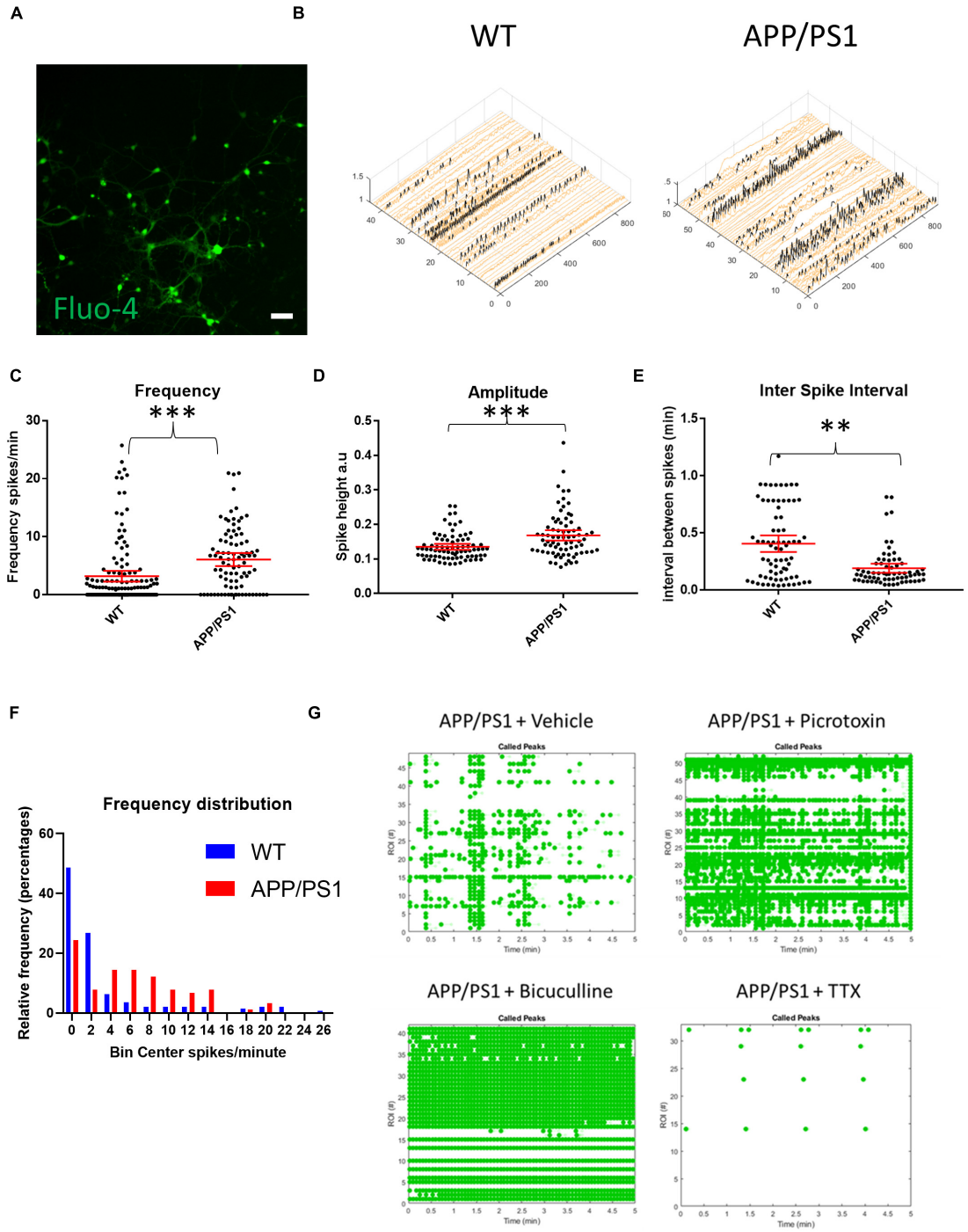

FIGURE 1 | Increased spontaneous activity in APP/PS1 primary neurons. **(A)** Representative micrograph of cultured neurons loaded with Fluo4. **(B)** Representative calcium traces from WT and APP/PS1 field of views (FOVs), black spikes are recognized by the Peakcaller algorithm. *X*-axis shows region of interest (ROI) number, *Y*-axis shows amplitude and *Z*-axis shows time point. **(C)** Frequency of firing (spikes per minute) is increased in APP/PS1 compared to WT neurons (APP/PS1 mean = 6.072, CI = 4.948–7.197, $n = 90$ compared to WT mean = 3.184, CI = 2.25–4.118, $n = 142$, $p < 0.0001$). **(D)** Amplitudes of spikes are increased in APP/PS1 compared to WT neurons (APP/PS1 mean = 0.1682, CI = 0.1532–0.1833, $n = 76$, compared to WT mean = 0.1352, CI = 0.1266–0.1437, $n = 80$, $p = 0.0003$). **(E)** Inter-spike interval distributions differ between APP/PS1 compared to WT neurons with more of the APP/PS1 neurons having low inter-spike intervals ($p = 0.0011$ using Kolmogorov–Smirnoff test). **(F)** Frequency distribution of firing frequencies of APP/PS1 compared to WT neurons shown in a graph; note higher percentage of WT neurons in the inactive bins; WT inactive = 69, APP/PS1 inactive = 22, WT active = 73 and APP/PS1 active 68, $p = 0.0003$, Fisher's exact test; $N = 4$ cultures. **(G)** Representative Raster plot of APP/PS1 neurons treated with vehicle (sterile milliQ water), 10 μM of picrotoxin, 20 μM of bicuculline or 1 μM of tetrodotoxin (TTX); neurons were imaged every 100 ms for 5 min with detected spikes represented as green dots. Mann–Whitney *U* test; $^{**}p < 0.01$, $^{***}p < 0.001$; scale bar: 50 μm.

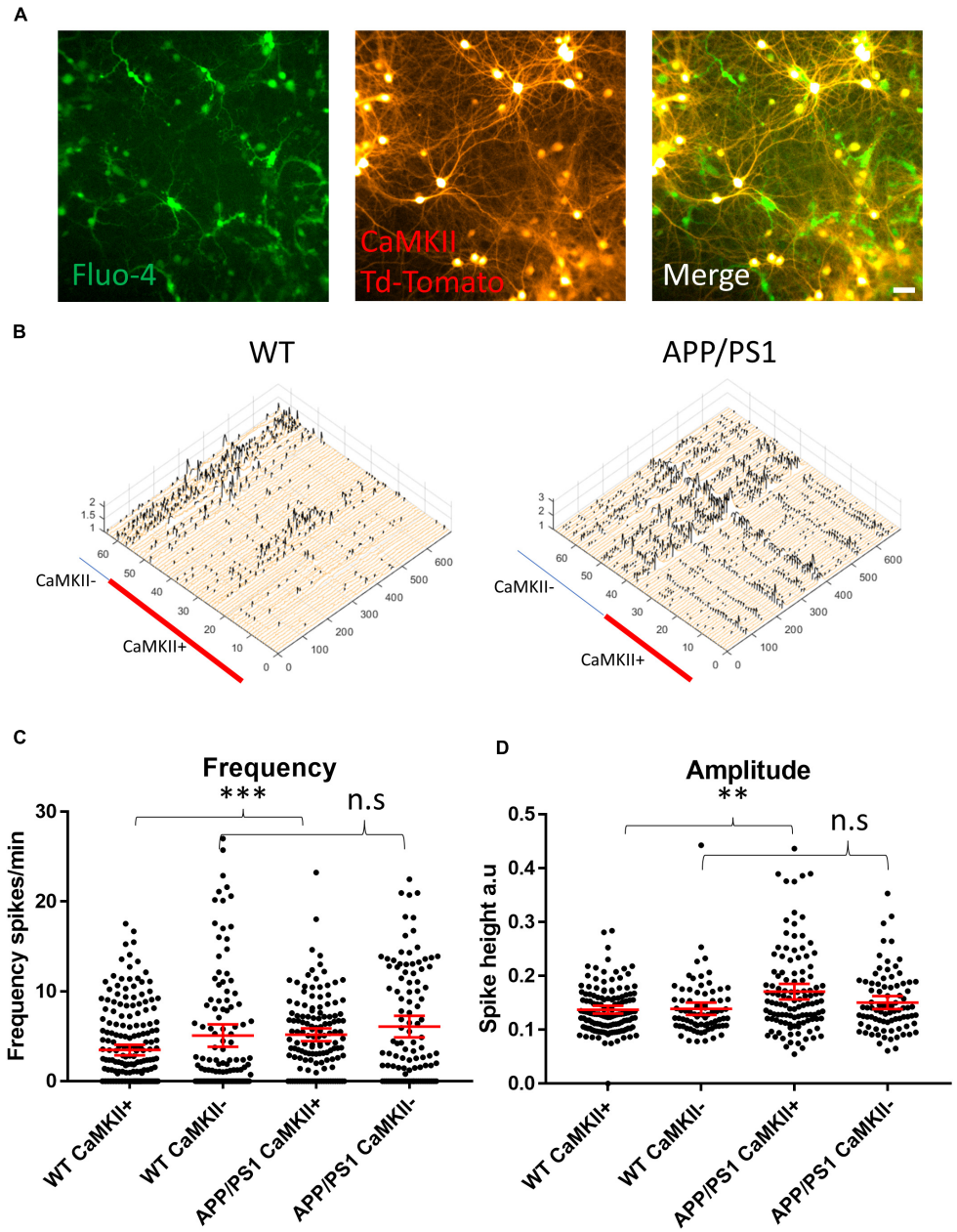

FIGURE 2 | Increased amplitude and frequency of spontaneous calcium transients in CaMKII positive excitatory neurons. **(A)** Micrograph provides an example of an image of Fluo-4 (green) and CaMKII TdTomato (red) neurons in culture. **(B)** Representative calcium traces from WT and APP/PS1 FOVs, black spikes are recognized by the Peakcaller algorithm. *X*-axis shows ROI number, *Y*-axis shows amplitude and *Z*-axis shows time point. The red line shows which ROIs belonged to CaMKII positive neurons in the representative FOVs. **(C)** Graph showing increase in spike frequency (spikes per minute) of APP/PS1 CaMKII positive compared to WT CaMKII positive neurons (APP/PS1 mean = 5.176, CI = 4.456–5.896, $n = 133$ compared to WT mean = 3.479, CI = 2.9–4.057, $n = 205$, $p = 0.0001$). In contrast, spike frequency of CaMKII negative APP/PS1 neurons did not significantly differ from WT CaMKII negative neurons (APP/PS1 mean = 6.094, CI = 4.898–7.291, $n = 108$ compared to WT mean = 5.083, CI = 3.837–6.328, $n = 114$, $p = 0.124$). **(D)** Amplitude of transients is increased specifically in APP/PS1 compared to WT CaMKII positive excitatory neurons (APP/PS1 mean = 0.171, CI 0.1566–0.1856, $n = 115$, compared to WT mean = 0.1375, CI = 0.1304–0.1446, $n = 138$, $p = 0.0024$). In contrast, the amplitude of transients in CaMKII negative neurons did not differ between APP/PS1 and WT neurons (APP/PS1 mean = 0.1505, CI = 0.1385–0.1625, $n = 85$, compared to WT mean = 0.1391, CI = 0.1275–0.1506, $n = 78$, $p = 0.302$); $N = 3$. Kruskal–Wallis test with Dunn's correction for multiple comparisons. n.s = not significant, $^{*}p < 0.05$, $^{**}p < 0.01$, $^{***}p < 0.001$; scale bar: 50 μm.

Likewise, analyses of neurons immunolabelled for glutamatergic (VGluT and CaMKII) and GABAergic (vGAT and gephyrin) synaptic markers using the image analysis plugins NeuronJ and Synapcount (Mata et al., 2017) did not show significant differences between APP/PS1 and WT cultures (**Figures 3D–F**). Similarly, counting CaMKII positive cells as a percentage of

all MAP2 positive cells per culture did not show a significant difference between the percentage of CaMKII neurons in WT and APP/PS1 neuronal cultures (**Figure 3G**). However, consistent with prior work (Siskova et al., 2014), our analyses did show decreased dendritic length in APP/PS1 compared to WT neurons (**Figures 3H,I**).

Individual Contributions of Amyloid Precursor Protein and Aβ to Neuronal Hyperactivity

To dissect out the individual role of APP on neuronal activity, we investigated whether APP over-expression alone without a concomitant elevation in Aβ could cause hyper-activity by transducing WT neurons with constructs encoding either mutant human APP resistant to BACE cleavage (hAPPmv) (Kamenetz et al., 2003) or WT human APP (hAPPwt), both under a CaMKII promoter. Remarkably, the expression of either APP construct in WT neurons led to an increase in the frequency and amplitude of calcium transients (**Figures 4A,B**), indicating an Aβ-independent effect of APP on neuronal activity in excitatory neurons.

Likewise, we sought to investigate whether increased Aβ levels alone could induce hyper-activity. We wanted to increase Aβ levels in WT cultures without affecting APP and PS1 as this could confound our results, since we provide evidence that overexpression of APP has Aβ-independent effects on neuronal activity, while PS1 has been shown to alter calcium signaling (Lerdkrai et al., 2018). Therefore, we utilized an inhibitor of the Aβ degrading enzyme neprilysin, which increases Aβ levels (Abramov et al., 2009), primarily at synapses, as neprilysin is highly expressed pre-synaptically (Iwata et al., 2004; Abramov et al., 2009). After 1 h of treatment with the neprilysin inhibitor thiorphan (500 nM), calcium transient frequencies (**Figure 4C**) and amplitudes (**Figure 4D**) were increased in WT primary neurons. Interestingly, thiorphan led to a greater increase in firing frequency in CaMKII-positive compared to CaMKII-negative neurons (**Figure 4E**). As neprilysin also degrades other peptides, such as substance P and neurokinin A, as a control, we assessed the effect of thiorphan treatment on APP knockout (KO) neurons, which lack APP and, thus, the capacity to generate Aβ. Indeed, calcium transient frequencies and amplitudes from APP KO neurons treated with thiorphan did not significantly differ from APP KO neurons treated with vehicle alone (**Figure 4F**), supporting the conclusion of elevated Aβ levels as driving the hyperactivity in WT neurons treated with thiorphan. However, APP KO neurons have been shown to have altered synaptic composition (Martinsson et al., 2019) and calcium transients (Yang et al., 2009), which could potentially mask effects by thiorphan. Therefore, as an alternative to investigate elevated Aβ levels on hyperactivity, we added exogenous synthetic Aβ peptide to WT cultures.

Immunolabeling WT neuronal cultures treated with 0.5 μM of synthetic human Aβ1–42 for 2 h with the human-specific Aβ/APP antibody 6E10 showed that the added exogenous Aβ1–42 localized to the dendritic spines of CaMKII-TdTomato expressing neurons (**Figures 5A,B**). This was consistent with prior findings showing that exogenous Aβ1–42 preferentially binds to synapses of CaMKII-immunoreactive neurons (Willen et al., 2017). Interestingly, we detected marked colocalization of the added human Aβ1–42 with the fibril and fibrillar oligomer-specific antibody OC that detects amyloid structures (Hatami et al., 2014), indicating aggregation of the exogenous Aβ1–42 at synapses, which is consistant with prior work (Willén et al., 2017). While for these experiments we added supraphysiological levels of Aβ1–42 (0.5 μM), in order to more readily visualize its localization, we next assayed what effect more physiological Aβ1–42 increases would have on calcium oscillations. Given that physiological levels of Aβ are in the picomolar range and that picomolar levels of exogenous Aβ were reported to increase LTP (Puzzo et al., 2008), we added 200 pM of synthetic human Aβ1–42 acutely to mouse WT neuronal cultures expressing CaMKII-driven TdTomato. Addition of 200 pM synthetic Aβ to WT cultures led to modest increases in the firing frequencies of both CaMKII-positive and CaMKII-negative neurons (**Figure 5C**). In addition, these picomolar levels of Aβ1–42 led to increased amplitudes of calcium oscillations in CaMKII-positive neurons but not CaMKII-negative neurons (**Figure 5D**). However, higher concentrations of synthetic Aβ1–42 (500 nM) did not lead to significantly increased calcium oscillations (**Figure 5E**), though 500 nM of synthetic Aβ1–40 did lead to a robust increase in firing frequency. In summary, our results support the concept that APP and Aβ can independently induce increases in synaptic activity, which likely plays a role under physiological and pathological conditions.

Dysregulated Homeostatic Plasticity in Amyloid Precursor Protein/PS1 Neurons

Since we showed that elevating either APP or Aβ in WT neurons can increase neuronal activity, we hypothesized that the continuously high levels of APP and Aβ in APP/PS1 neurons disrupt neuronal network activity and function, and speculated that HSP mechanisms, which help maintain synaptic firing within the boundaries of meaningful communication (Turrigiano, 2008), might be impaired in AD transgenic neurons and, as a result, may no longer be effective at returning activity levels back to a baseline. Dysfunctional HSP could explain part of the sustained hyperexcitability observed in neurons from AD transgenic mouse models. We therefore hypothesized that long-term high levels of Aβ/APP might impair homeostatic plasticity. This can be tested by manipulating neuronal firing outside of a network's set point, leading to plasticity changes that maintain the baseline activity level. We therefore initially treated APP/PS1 and WT neurons with TTX and bicuculline, which should immediately decrease network activity and increase network activity, respectively (Turrigiano et al., 1998). Indeed, acute treatment of WT and APP/PS1 neurons with TTX and bicuculline led to the expected decreased and increased activity, respectively (**Supplementary Figures 1E,F**). Next we treated WT and APP/PS1 neurons with TTX or bicuculline for a longer period of time (48 h), which are established methods for inducing HSP (Turrigiano et al., 1998). Interestingly, 48 h of TTX treatment led to a sharp decrease by western blot in total APP protein levels in both WT and APP/PS1 neurons (**Figures 6A,B**),

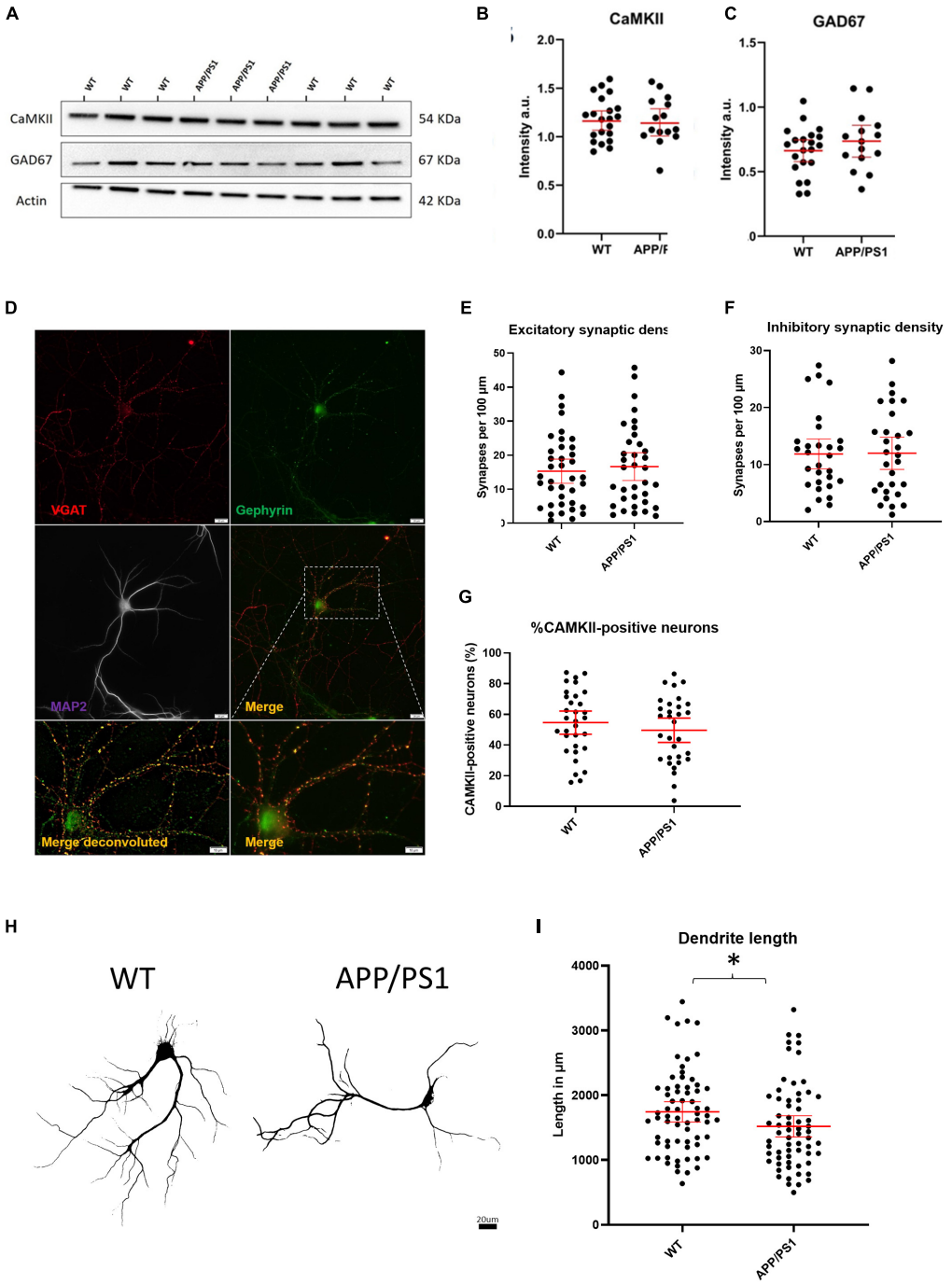

FIGURE 3 | No evidence for gross imbalances in excitatory/inhibitory neurons/synapses in APP/PS1 compared to WT neurons. **(A)** Representative western blot of CaMKII and GAD67 protein levels with actin as loading control. **(B)** Quantification of western blot of CaMKII in **(A)** (APP/PS1 mean = 1.164, CI = 1.030–1.298, n = 15 and WT mean = 1.181, CI = 1.080–1.282, n = 21, p = 0.8270). **(C)** Quantification of western blot of GAD67 in **(A)** (APP/PS1 mean = 0.7359, CI = 0.6129–0.8589, n = 15 and WT mean = 0.6620, CI = 0.5774–0.7466, n = 21, p = 0.2860, unpaired t-test). **(D)** Representative micrograph showing WT neuron labeled with VGAT (red), Gephyrin (green) and MAP2 (magenta). Lower panels show an enlarged view of neuron both with (left) and without (right) deconvolution. Scale bar = 20 µm and for Merge, 10 µm. **(E)** Graph depicting excitatory synaptic density from VGLUT/CAMKII overlap divided by neurite length (APP/PS1 mean = 16.64., CI = 12.53–20.74, n = 35 and WT mean = 15.28, CI = 11.74–18.83, n = 38, p = 0.6129, unpaired t-test). **(F)** Graph depicting inhibitory synaptic density from VGAT/Gephyrin overlap divided by neurite length (APP/PS1 mean = 12.00, CI = 9.160–14.84, n = 29 and WT mean = 11.87, CI = 9.243–14.50, n = 29 p = 0.9458). **(G)** Graph depicting quantification of percentage CaMKII neurons in WT and AD cultures. (APP/PS1 mean = 49.61% CaMKII positive neurons CI = 41.67–57.54% compared to WT mean = 54.64% CI = 47.08–62.14%, p = 0.35, unpaired t-test). **(H)** Representative binary images of WT and APP/PS1 neurons labeled for MAP2; scale bar = 20 µm. **(I)** Graph showing decreased dendrite length in APP/PS1 compared to WT neurons (APP/PS1 mean = 1518, CI = 1355–1682, n = 64, and WT mean = 1744, CI = 1588–1900. N = 67, p = 0.045, unpaired t-test). *p < 0.05.

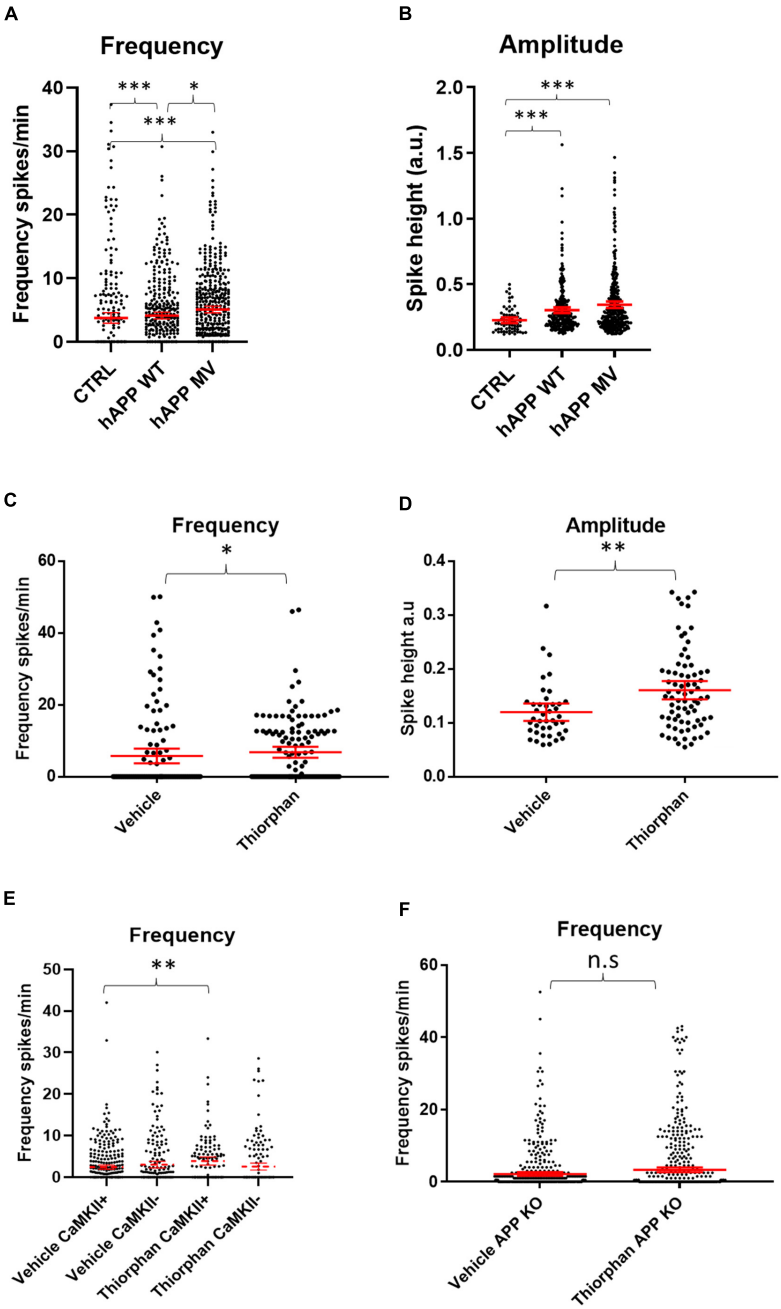

FIGURE 4 | Amyloid precursor protein and Aβ increase calcium oscillation frequency and amplitude. **(A)** Graph depicts firing frequencies in WT neurons transduced with a viral vector harboring hAPPwt or hAPPmv (BACE cleavage resistant) under a CaMKII promoter. Note that both hAPPwt and hAPPmv increase the firing frequency compared to control (CTRL), with hAPPmv having a stronger effect [hAPPmv mean = 5.087, CI = 4.542–5.633, n = 436; hAPPwt mean = 4.112, CI = 3.585–4.640, n = 375 and CTRL mean = 3.757, CI = 2.925–4.588, n = 292, p-values respective to CTRL = hAPPmv = 0.0001, hAPPwt = 0.0001, p-value hAPPmv compared to hAPPwt (p = 0.0259), Kruskal–Wallis Dunn's correction]. **(B)** Graph showing increased amplitude in neurons expressing hAPPwt and hAPPmv under CaMKII promoter (hAPPmv mean = 0.3444, CI = 0.3197–0.3691, n = 344 and hAPPwt mean = 0.3021, CI = 0.2808–0.3433, n = 278 and CTRL mean = 0.2256, CI = 0.2034–0.2479, n = 67, N = 3, p-values respective to CTRL; hAPPmv = 0.0001, hAPPwt = 0.0004, p-value, Kruskal–Wallis Dunn's correction). Kruskal–Wallis test with Dunn's correction for multiple comparisons. **(C)** WT neurons treated with 500 nM of the neprilysin inhibitor thiorphan for 1 h show increased firing frequency (thiorphan mean = 6.814, CI = 5.283–8.344, n = 133, compared to vehicle mean = 5.783, CI = 3.749–7.817, n = 125, N = 3, p = 0.0101). **(D)** The graph depicts increased spike amplitudes after 1 h of treatment of WT neurons with thiorphan (thiorphan mean = 0.1605, CI = 0.1436–0.1774, n = 76, compared to vehicle mean = 0.1198, CI = 0.1036–0.136, n = 42, p = 0.0012). **(E)** Graph showing increase in spike frequency of thiorphan treated CaMKII positive compared to vehicle treated CaMKII positive neurons (thiorphan mean = 3.905, CI = 2.942–4.869, n = 128 compared to vehicle mean = 2.432, CI = 1.934–2.931, n = 332, N = 3, p = 0.0089). In contrast, spike frequency of CaMKII negative thiorphan treated neurons did not significantly differ from vehicle treated CaMKII negative neurons (thiorphan mean = 2.566, CI = 1.726–3.406, n = 173 compared to vehicle mean = 3.018, CI = 2.243–3.794, n = 218, p = 0.0894). **(F)** Graph showing that thiorphan was ineffective at inducing increased frequency in APP KO neurons compared to vehicle (APP KO thiorphan mean = 3.329, CI = 2.692–3.967, n = 601 compared to APP KO vehicle mean = 2.196, CI = 1.689–2.704, n = 514, N = 3, p = 0.8604, Mann–Whitney U-test).; n.s = not significant, *$p < 0.05$, **$p < 0.01$, ***$p < 0.001$.

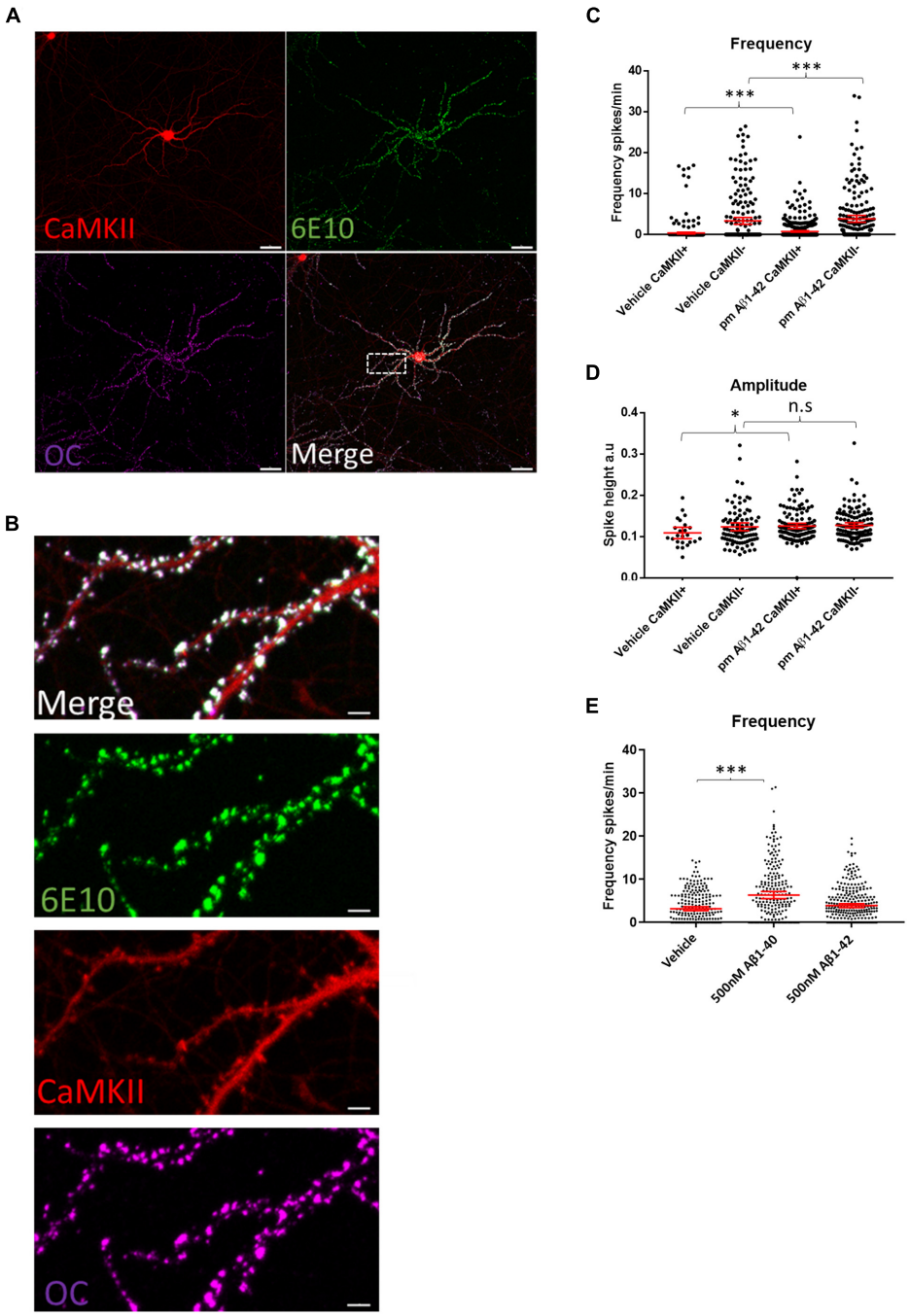

FIGURE 5 | Aβ preferentially binds synaptic compartments on CaMKII positive neurons and appears to have a dose dependent effect on spike frequency. **(A)** Micrograph showing that synthetic human Aβ1–42 preferentially binds to dendrites of CaMKII positive murine WT neurons; Td Tomato expressed through CaMKII promoter, human specific anti-Aβ antibody 6E10 (green) and conformation specific anti-amyloid antibody OC (magenta); scale bar = 50 μm. **(B)** Insert from **(A)** showing Aβ1–42 targeting synapses; note that antibody 6E10 labels the added synthetic human Aβ and that this is also labeled by the fibrillar oligomer antibody OC; scale bar = 5 μm. **(C)** WT neurons treated with 200 pM synthetic Aβ1–42 show increased spike frequency compared to DMSO treated vehicle control neurons both in CaMKII positive neurons (Aβ1–42 mean = 0.7554, CI = 0.5724–0.9383, n = 477, compared to vehicle mean = 0.367, CI = 0.1636–0.5704, n = 401, $p < 0.0001$) and in CaMKII negative neurons (Aβ1–42 mean = 3.829, CI = 3.033–4.685, n = 214, compared to vehicle mean = 3.346, CI = 2.508–4.183, n = 218). **(D)** Graph depicting increased amplitudes in CaMKII positive neurons treated with 200 pM Aβ1–42 compared with DMSO vehicle control (Aβ1–42 mean = 0.1256, CI = 0.119–0.1321, n = 128, compared to vehicle mean = 0.1087, CI = 0.09495–0.1225, n = 24, p = 0.045). However, CaMKII negative neurons did not show a significant increase in amplitude with Aβ treatment (Aβ1–42 mean = 0.1272, CI = 0.1209–0.1334, n = 133, compared to vehicle mean = 0.1235, CI = 0.114–0.133, n = 94, p = 0.2103). **(E)** Graph shows WT neurons treated with 500 nM Aβ1–42 or 500 nM Aβ1–40. While 500 nM Aβ1–42 leads to a slight but not significantly different distribution of activity, Aβ1–40 strongly increases activity (Aβ1–40 mean = 6.344, CI = 5.503–7.186, n = 235 and Aβ1–42 mean = 3.901, CI = 3.439–4.363, n = 287 compared to vehicle mean = 3.194, CI = 2.752–3.635, n = 255; p = 0.0001 and p = 0.14.); Kruskal–Wallis test, N = 3. n.s = not significant, $^{*}p < 0.05$, $^{***}p < 0.001$.

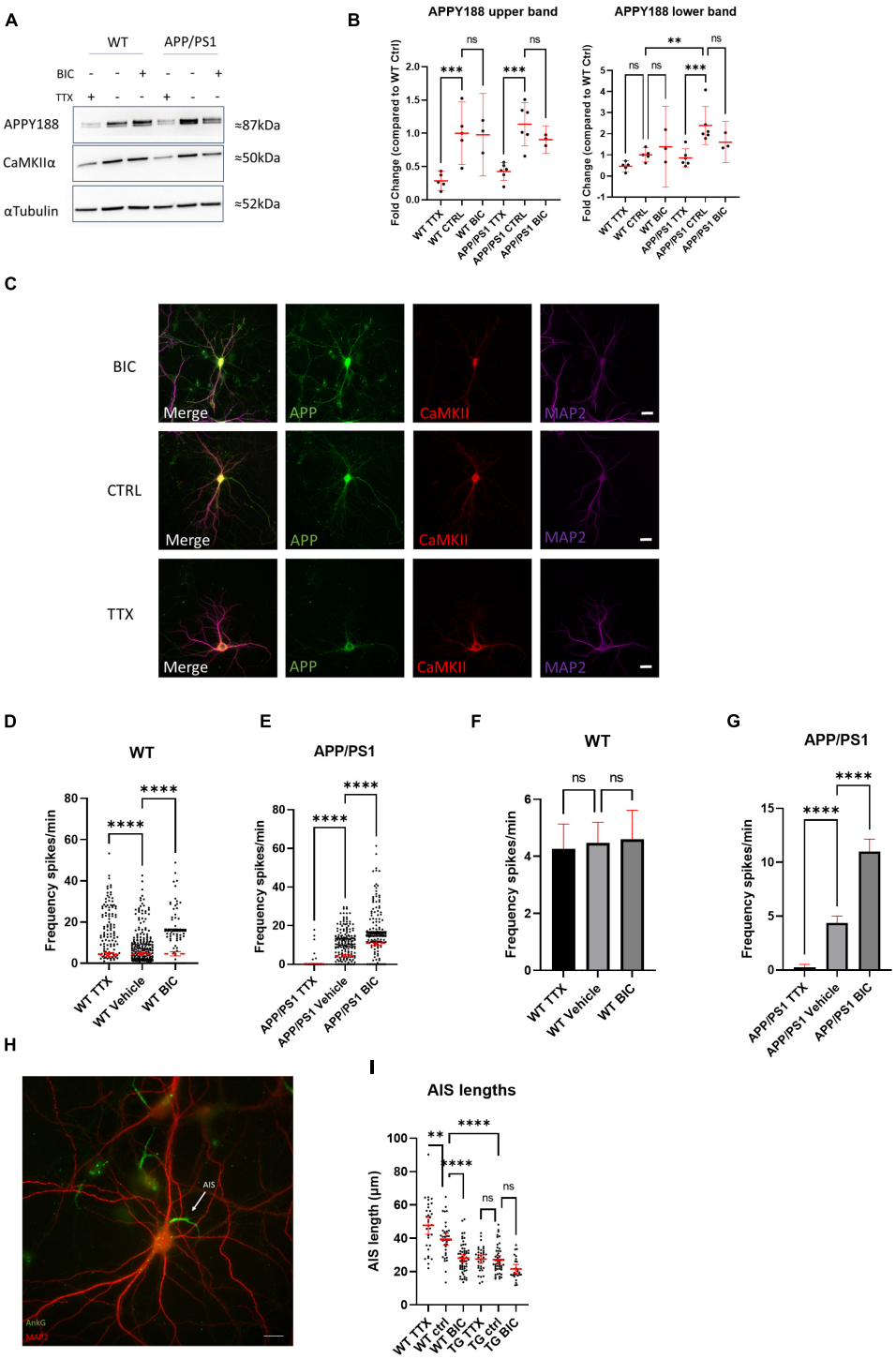

FIGURE 6 | Neurons from AD transgenic mice are unable to initiate homeostatic synaptic/intrinsic plasticity. **(A)** Representative western blot of APP (using antibody APPY188) and CaMKIIα in WT and APP/PS1 neurons treated with TTX or bicuculline for 48 h; αTubulin is used as a loading control. **(B)** Graph depicts quantification of fold change from western blots in **(A)**, APP upper band (WT TTX mean = 0.2865, CI 0.1287–0.4244, $n = 5$, WT control mean = 1.000, CI 0.5298–1.470, $n = 5$, WT bicuculline mean = 0.9782, CI 0.3574–1.599, $n = 3$, APP/PS1 TTX mean = 0.4251, CI 0.2893–0.5609, $n = 6$, APP/PS1 control mean = 1.137, CI 0.8116–1.462, $n = 6$, APP/PS1 bicuculline mean = 0.9038, CI 0.6975–1.110, $n = 3$) and the fainter APP lower band (WT TTX mean = 0.4605, CI 0.1990–0.7220, $n = 5$, WT control mean = 1.000, CI 0.6601–1.340, $n = 5$, WT bicuculline mean = 1.386, CI –0.5278–3.299, $n = 3$, APP/PS1 TTX mean = 0.8590, CI 0.4258–1.292, $n = 6$, APP/PS1 control mean = 2.239, CI 1.493–3.290, $n = 6$, APP/PS1 bicuculline mean = 1.602, CI 0.6279–2.576, $n = 3$). Note that the upper APP band is lower in TTX treated WT compared to WT control ($p = 0.0006$) and TTX treated APP/PS1 compared to APP/PS1 control ($p = 0.0002$). For the APP lower band, it was significantly higher in the APP/PS1 control than the WT control ($p = 0.0017$), while APP was lower in the APP/PS1 TTX than the APP/PS1 control ($p = 0.0003$; one-way ANOVA, Šidak

(Continued)

FIGURE 6 | correction). **(C)** Micrograph showing APP and CaMKIIα labeling after 48 h of TTX or bicuclline treatment. Note that APP labeling is relatively weaker in the TTX treated neuron consistent with the results from western blot. Scale bar = 20 μm. **(D)** Graph demonstrating HSP adaptations in WT cultures treated with TTX or bicuculline for 48 h. Note that the distribution of oscillation frequency in bicuculline treated neurons is different compared to vehicle treated (TTX mean = 4.265, CI 3.397–5.134, n = 442; vehicle mean = 4.467, CI = 3.741–5.192, n = 413; bicuculline mean = 4.593, CI = 3.574–5.611, n = 303, p-values compared to vehicle: TTX = 0.0001 and bicuculline = 0.0001, Kruskal–Wallis test, N = 4). **(E)** Graph showing absence of adaptation in APP/PS1 neurons in response to 48 h of TTX or bicuculline treatment. Note how both TTX or bicuculline treated APP/PS1 neurons are largely opposite from WT neurons after 48 h. (TTX mean = 0.272, CI 0.0154–0.527, n = 210; vehicle mean = 4.368, CI = 3.729–5.008, n = 464; bicuculline mean = 10.990, CI = 9.835–12.140, n = 368, p-values compared to vehicle: TTX = 0.0001 and bicuculline = 0.0001, Kruskal–Wallis test, N = 4). **(F)** Bar graph showing mean firing frequency from **(D)**; note that mean firing frequencies are similar between the groups. (WT TTX vs. WT vehicle p = 0.9203, WT bicuculline vs. WT vehicle, p = 0.9733, one-way ANOVA, Dunnett's test). **(G)** Bar graph showing mean firing frequency from **(E)**; note that mean firing frequencies are do not recover as in WT. (APP/PS1 TTX vs. APP/PS1 vehicle p = 0.0001, APP/PS1 bicuculline vs. APP/PS1 vehicle, p = 0.0001, one-way ANOVA, Dunnett's test). **(H)** Micrograph depicting WT neuron labeled with MAP2 (red) and ankyrin-G (green), which labels the AIS. White arrow points to AIS; scale bar = 20 μm. **(I)** Graph shows quantification of AIS lengths after treatment with TTX or bicuculline for 48 h (WT TTX mean = 47.76, CI = 42.36–53.17, n = 32; WT vehicle mean = 39.44, CI = 35.87–43.02, n = 37; WT bicuculline mean = 28.07, CI = 25.75–30.39, n = 57; APP/PS1 TTX mean = 27.52, CI = 25.01–30.04, n = 35; APP/PS1 vehicle mean = 27.20, CI = 24.85–29.55, n = 49; APP/PS1 bicuculline mean = 21.57, CI = 18.86–24.27, n = 26); ordinary one way ANOVA, Tukey's multiple comparisons test. ns = not significant, $^{*}p < 0.05$, $^{***}p < 0.001$, $^{****}p < 0.0001$.

in particular in the upper band, which corresponds to mature APP, as visualized by the APPY188 antibody. Although a similar trend was seen for the lower, immature APP band this did not reach statistical significance. The decrease in APP levels was also evident in WT primary neuron cultures immunolabelled after 48 h treatment with TTX or Bicuculline (**Figure 6C**). There was also a trend for a decrease in CaMKIIα, which was previously reported to be downregulated with TTX induced homeostatic scaling (Thiagarajan et al., 2002). To determine whether HSP mechanisms were induced by the long-term treatments, we measured the calcium transients after HSP induction. Treating WT neurons with TTX or bicuculline for 48 h led to the expected changes in excitability; most TTX treated WT neurons recover their ability to fire and while the distribution of firing rates is altered (**Figure 6D** and **Supplementary Figures 2A,B**), the mean firing frequency does not differ significantly from WT vehicle treated neurons after 48 h (**Figure 6F**). In response to the 48 h of treatment with bicuculline, which acutely elevates activity, most WT neurons, as expected, significantly decreased their firing frequency. Of note, the extended bicuculline treatment in WT neurons appears to lead to two types of firing, with one group of neurons maintaining a high firing frequency and another group that is silent (**Figures 6D,F**). In contrast, the firing frequency of APP/PS1 neurons treated for 48 h with bicuculline remained increased, while the firing frequency of APP/PS1 neurons after chronic TTX treatment remained low (**Figures 6E,G**). Thus, APP/PS1 neurons did not respond to the prolonged bicuculline or TTX exposure as the WT neurons, indicating that the APP/PS1 neurons were unable to compensate to these pharmacologically-induced changes in neuronal activity. Note that vehicle treated APP/PS1 and WT were not significantly different in this experiment although here we did not do direct comparisons.

To explore a mechanistic aspect of these HSP alterations we investigated axon initial segment (AIS) modifications in the chronic TTX and bicuculline treated cultures, as lengthening or shortening of the AIS modifies the excitability of neurons. By immunolabeling for ankyrin-G, a protein involved in linking voltage-gated channels to the AIS, we could identify the AIS and measure its length (Hedstrom et al., 2008). In WT neurons, 48 h of treatment with either bicuculline or TTX led to the expected decreased and increased AIS lengths, respectively (**Figures 6H,I**). In contrast, APP/PS1 neurons did not display adjustments of the AIS length upon either of these HSP-inducing treatments. Interestingly, the AIS lengths of APP/PS1 neurons were already shorter than those of WT neurons at baseline. Together these experiments demonstrate an inability of APP/PS1 neurons to use HSP mechanisms to adapt to extrinsic changes in activity.

DISCUSSION

Here we demonstrate that inhibition of Aβ degradation, application of synthetic Aβ, APP overexpression and familial AD-causing mutations all cause an increase in somatic calcium transients during spontaneous neuronal activity, in particular in excitatory CaMKII positive neurons. Moreover, we present evidence that homeostatic plasticity mechanisms are disrupted in APP/PS1 AD transgenic neurons, as these were unable to compensate their spontaneous calcium transient activity after chronic activity or inactivity. APP/PS1 neurons were shown to have shorter AIS and a lack of change in AIS length in response to chronic activity or chronic activity blockade. The proper function of neuronal networks depends on maintaining homeostatic set points and limiting activity within functional windows. Deviations from these set-points lead to network dysfunction. Structural homeostatic synaptic plasticity is known to occur at three main locations: (1) at the post-synapse involving reduced or increased levels of surface receptors (Turrigiano et al., 1998); (2) at the axon initial segment (AIS) by either increasing or decreasing its length or by shifting the AIS further out into the axon (Wefelmeyer et al., 2016); or (3) at the pre-synapse by modifying how much neurotransmitter is stored in synaptic vesicles or through homeostatic maintenance of presynaptic exocytosis (Delvendahl et al., 2019). Of note, Aβ was suggested to overshoot normal homeostatic scaling in response to sensory deprivation *in vivo* or TTX-mediated inhibition *in vitro* (Gilbert et al., 2016), and Aβ was recently shown to regulate homeostatic synaptic upscaling after activity blockade in dentate gyrus *in vivo* (Galanis et al., 2021). Our findings that APP/PS1 neurons do not increase their activity after 48 h of TTX treatment nor decrease firing rate after 48 h of bicuculline treatment suggest that Aβ/APP play important roles

not only in adjusting to activity blockade but also have roles in homeostatic downscaling in response to excessive activity. Interestingly, we found that 48 h of bicuculline treatment led to a strong reduction in firing in the majority of neurons in WT cultures with, however, another population of neurons that maintained a high firing frequency; a related observation was reported on visual cortex homeostatic plasticity following visual deprivation (Barnes et al., 2015), where differential adaptations by excitatory and inhibitory neuron populations were described. Interestingly, we observed that the mean firing rates were similar between TTX, vehicle and bicuculline treated WT neurons after 48 h consistent with findings suggesting that while single unit firing is unstable, networks maintain surprisingly stable firing frequencies (Slomowitz et al., 2015). Aβ and APP have been implicated in normal HSP (Gilbert et al., 2016; Galanis et al., 2021), and APP/PS1 mice were recently shown to have defective downscaling during sleep (Zarhin et al., 2022). Defective HSP could help explain why AD transgenic mice are more susceptible to pharmacologically-induced and spontaneous seizures (Minkeviciene et al., 2009; Reyes-Marin and Nuñez, 2017) and could provide a framework for explaining the increased sensitivity to seizures in AD patients (Pandis and Scarmeas, 2012).

We provide evidence that the AIS is lengthened with TTX treatment and shortened after treatment with bicuculline in WT neurons, which, however, did not occur in APP/PS1 neurons. Shortening the AIS is a way to decrease intrinsic excitability and previous work in slice cultures has shown that 1 h of bicuculline treatment was sufficient to decrease the length of the AIS (Jamann et al., 2021). Since the average lengths of the AIS in APP/PS1 neurons are shorter at baseline than in WT neurons, and are not altered by chronic treatments known to induce HSP, our findings could indicate that APP/PS1 neurons have attempted to adapt to reduce excitability (reduced baseline AIS) but are unable to do so to treatments that normally would induce HSP. It should be noted, however, that the shortening of the AIS occurs within 1 h while complete downscaling takes closer to 48 h. Thus, the role of the AIS shortening in the regulation of activity in APP/PS1 neurons is likely minor. We previously showed in primary neurons from Tg2576 AD transgenic mice, which overexpress human APP with the Swedish familial AD mutation, reduced AMPA receptor levels in culture (Almeida et al., 2005). Whether this is the result of adaptation to higher basal activity levels or a consequence of synaptotoxicity remains to be determined. Moreover, we demonstrate here that APP protein levels decrease with chronic TTX treatment. It has been previously reported that conditional APP family triple knockout increases excitability of excitatory neurons (Lee et al., 2020). Thus, the reduction we see in APP protein levels could be related to increasing excitability in the chronic TTX treatment as we also demonstrated in a previous paper that APP knockout and knockdown led to increased GluA1 protein levels both in cultured neurons and brains of APP KO mice (Martinsson et al., 2019). However, while TTX decreased levels of APP, bicuculline treatment did not significantly alter APP levels.

Our data demonstrates hyperexcitability in APP/PS1 transgenic compared to WT neurons, which we now show occurs mainly in excitatory neurons. Similar to previous studies, we found that exogenously added Aβ1–42 primarily targeted synapses of CaMKII-positive neurons, specifically in a dendritic rather than axonal pattern (Lacor et al., 2004; Willen et al., 2017). However, this does not exclude the possibility of Aβ binding to presynaptic terminals proximal to dendrites. The binding of Aβ1–42 to CaMKII-positive synapses might explain why excitatory neurons, in particular, are affected. The increased frequencies and amplitudes of calcium oscillations that we observed with neprilysin inhibition as a means to elevate endogenous Aβ are consistent with results from Abramov et al. (2009), showing increased release probability with thiorphan treatment in cultured hippocampal neurons. However, since neprilysin also degrades various enkephalins and peptide neurotransmitters, such as substance P, which can influence calcium stores (Heath et al., 1994), we additionally showed a lack of effect on calcium oscillations with neprilysin inhibition in APP KO neurons.

As the calcium oscillations were increased in APP/PS1 compared to wild type neurons, we also considered whether this might be due to decreased inhibitory interneurons/synapses. However, we did not see significant differences in the protein levels of GAD67 and CaMKII, markers of GABAergic interneurons and excitatory neurons, respectively. Further, we did not detect significant differences in the synaptic density of either excitatory or inhibitory synapses. While neuropathological studies have emphasized the vulnerability of select classes of excitatory projection neurons (Stranahan and Mattson, 2010), the relative involvement of different inhibitory and excitatory neurons in early Aβ-induced hyperactivity remains less well defined. However, while there is no evidence for differences in the proportion of different subclasses of neurons in cortical versus hippocampal neurons of AD transgenic versus WT primary cultures, we also cannot exclude this possibility. Increasing evidence suggests that alterations in inhibitory neuron connectivity lead to changes in network functions in AD. For example, increased parvalbumin and gephyrin labeling perisomatically in CA1 neurons of young APP/PS1 transgenic mice was shown (Hollnagel et al., 2019), which might represent an adaptation to increased Aβ/APP and, therefore, increased activity in these mice.

Cortical neurons in proximity to plaques were reported to have higher basal calcium levels in spines and dendrites (Kuchibhotla et al., 2008). Aβ oligomers of different varieties have been reported to bind various cell surface receptors such as PrP (Lauren et al., 2009), alpha7 nicotinic receptor (Sadigh-Eteghad et al., 2014), NMDA receptors (Texidó et al., 2011), and Ephrins (Vargas et al., 2018), leading to an influx of calcium. Yet another hypothesis proposes that Aβ increases the cell membrane permeability for calcium (Kawahara and Kuroda, 2000; Kagan et al., 2002). To complicate matters, presenilins have also been implicated in the handling of Ca^{2+} stores independently of γ-secretase in AD transgenic mouse models (Lerdkrai et al., 2018). A recent study suggested that Aβ dimers could cause hyperactivity by inhibiting glutamate reuptake (Zott et al., 2019).

Further, it was reported that Aβ oligomers can impair synaptic activity by repressing P/Q calcium channels (Nimmrich et al., 2008). While we prepared synthetic Aβ in DMSO, which prevents the formation of fibrils, Aβ forms amyloids with time in culture (Takahashi et al., 2004) and progressively aggregates at synapses (Takahashi et al., 2002, 2004; Willén et al., 2017), consistent with Aβ aggregation at synaptic compartments (Bilousova et al., 2016). Moreover, while Aβ and APP influence synaptic activity, neuronal activity also regulates APP cleavage and Aβ generation (Kamenetz et al., 2003); increased neuronal activity can increase both the generation and degradation of Aβ (Kamenetz et al., 2003; Tampellini et al., 2009). Thus, converging data indicate that both APP and Aβ are important for regulating neuronal activity. Among questions that remain to be answered are which specific aspects of neuronal activity APP and Aβ regulate/influence. Many transgenic models of AD exhibit epileptic seizures and hyperactivity (Scharfman, 2012; Born et al., 2014), and even models overexpressing wild-type human APP develop seizures (Born et al., 2014). Importantly, hyper-synchrony in AD transgenic mice could be rescued by genetic suppression of APP over-expression (Born et al., 2014). We hypothesize that the localization of APP and accumulating Aβ in endosomes near synapses (Takahashi et al., 2002) play a key role in the altered responses of synapses in the setting of AD. A better understanding of the neuron subtypes and molecular mechanisms involved in early Aβ/APP-induced hyperexcitability and synapse dysfunction should provide not only new insights into the disease, but also to new treatment strategies for AD.

DATA AVAILABILITY STATEMENT

The raw data supporting the conclusions of this article will be made available by the authors, without undue reservation, to any qualified researcher.

ETHICS STATEMENT

The animal study was reviewed and approved by Animal Ethical Committee at Lund University ethical permit number 5.8.18-05983/2019.

AUTHOR CONTRIBUTIONS

IM and GKG wrote and conceptualized the manuscript. IM, SCK, OS, and RE performed the experiments. IM, GKG, MGG, LT-G, and SCK edited the manuscript. IM, AS, OS, and RE performed the data analysis. LQ and CL performed cloning and prepared vectors. GKG, TD, and J-YL contributed funding to the project. All authors commented and edited the final version of the manuscript.

FUNDING

This study was supported by MultiPark, Hjärnfonden, Alzheimerfonden, Kockska stiftelsen, the Swedish Research Council (Grant #2019-01125), and the Olav Thon Foundation.

ACKNOWLEDGMENTS

We thank Bodil Israelsson for technical assistance as well as master's students Ainoa Pilkati and Mohammed Rahman for help with analyzing data. We appreciate the support of MultiPark, Hjärnfonden, Alzheimerfonden, Kockska stiftelsen, the Swedish Research Council (Grant #2019-01125), and the Olav Thon Foundation.

SUPPLEMENTARY MATERIAL

The Supplementary Material for this article can be found online at: https://www.frontiersin.org/articles/10.3389/fnagi.2022.946297/full#supplementary-material

Supplementary Figure 1 | Live-cell imaging method for assaying spontaneous calcium transients. **(A,B)** Representative traces of spontaneous activity over a 2 min period in neurons from WT and APP/PS1 mice, respectively. **(C,D)** Raster plots showing overall calcium transients (spikes represented as green dots) in WT and APP/PS1 neuron field of views (FOVs); ROI# or neuron number on the *Y*-axis and time in minutes on the *X*-axis. **(E)** Graph shows frequency from WT neurons treated with 1 μM TTX or 20 μM bicuculline. Note that TTX significantly reduces calcium oscillations whereas bicuculline significantly increases them compared to vehicle treated CTRL (TTX mean = 0.01429 CI = −0.01421–0.04278, $n = 70$; vehicle mean = 2.923, CI = 2.094–3.752, $n = 209$; bicuculline mean = 25.00, CI = 23.04–26.97, $n = 104$, p-values compared to vehicle: TTX = 0.0001 and bicuculline = 0.0001, Kruskal–Wallis test). **(F)** Graph demonstrating acute effects of TTX and bicuculline in APP/PS1 neurons. Note that similar to in WT neurons, TTX blocks activity while bicuculline raises activity (TTX mean = 0.1644 CI −0.07614–0.4050, $n = 118$; vehicle mean = 5.164, CI = 4.140–6.188, $n = 188$; bicuculline mean = 13.77, CI = 10.49–17.06, $n = 97$, p-values compared to vehicle: TTX = 0.0001 and bicuculline = 0.0379, Kruskal–Wallis test). $^{*}p < 0.05$, $^{***}p < 0.001$.

Supplementary Figure 2 | Frequency distribution of WT and APP/PS1 after 48 h treatment with TTX or bicuculline. **(A)** Frequency distribution of firing frequencies of WT neurons treated with TTX, bicuculline or vehicle for 48 h; neurons shown in a graph; $N = 3$ cultures. **(B)** Frequency distribution of firing frequencies of APP/PS1 neurons treated with TTX, bicuculline or vehicle for 48 h; neurons shown in a graph; $N = 3$ cultures.

REFERENCES

Abramov, E., Dolev, I., Fogel, H., Ciccotosto, G. D., Ruff, E., and Slutsky, I. (2009). Amyloid-β as a positive endogenous regulator of release probability at hippocampal synapses. *Nat. Neurosci.* 12:1567. doi: 10.1038/nn.2433

Almeida, C. G., Takahashi, R. H., and Gouras, G. K. (2006). Beta-amyloid accumulation impairs multivesicular body sorting by inhibiting the ubiquitin-proteasome system. *J. Neurosci.* 26, 4277–4288.

Almeida, C. G., Tampellini, D., Takahashi, R. H., Greengard, P., Lin, M. T., Snyder, E. M., et al. (2005). Beta-amyloid accumulation in APP mutant neurons reduces PSD-95 and GluR1 in synapses. *Neurobiol. Dis.* 20, 187–198. doi: 10.1016/j.nbd.2005.02.008

Artimovich, E., Jackson, R. K., Kilander, M. B. C., Lin, Y. C., and Nestor, M. W. (2017). PeakCaller: an automated graphical interface for the quantification of intracellular calcium obtained by high-content screening. *BMC Neurosci.* 18:72. doi: 10.1186/s12868-017-0391-y

Barnes, S. J., Sammons, R. P., Jacobsen, R. I., Mackie, J., Keller, G. B., and Keck, T. (2015). Subnetwork-specific homeostatic plasticity in mouse visual cortex *in vivo*. *Neuron* 86, 1290–1303. doi: 10.1016/j.neuron.2015.05.010

Bilousova, T., Miller, C. A., Poon, W. W., Vinters, H. V., Corrada, M., Kawas, C., et al. (2016). Synaptic amyloid-β oligomers precede p-tau and differentiate high pathology control cases. *Am. J. Pathol.* 186, 185–198. doi: 10.1016/j.ajpath.2015.09.018

Born, H. A., Kim, J. Y., Savjani, R. R., Das, P., Dabaghian, Y. A., Guo, Q., et al. (2014). Genetic suppression of transgenic APP rescues Hypersynchronous network activity in a mouse model of Alzeimer's disease. *J. Neurosci.* 34, 3826–3840. doi: 10.1523/JNEUROSCI.5171-13.2014

Delvendahl, I., Kita, K., and Müller, M. (2019). Rapid and sustained homeostatic control of presynaptic exocytosis at a central synapse. *Proc. Natl. Acad. Sci. U.S.A.* 116:23783. doi: 10.1073/pnas.1909675116

Doshina, A., Gourgue, F., Onizuka, M., Opsomer, R., Wang, P., Ando, K., et al. (2017). Cortical cells reveal APP as a new player in the regulation of GABAergic neurotransmission. *Sci. Rep.* 7:370. doi: 10.1038/s41598-017-00325-2

Faucher, P., Mons, N., Micheau, J., Louis, C., and Beracochea, D. J. (2016). Hippocampal injections of oligomeric Amyloid β-peptide (1–42) induce selective working memory deficits and long-lasting alterations of erk signaling pathway. *Front. Aging Neurosci.* 7:245. doi: 10.3389/fnagi.2015.00245

Galanis, C., Fellenz, M., Becker, D., Bold, C., Lichtenthaler, S. F., Müller, U. C., et al. (2021). Amyloid-beta mediates homeostatic synaptic plasticity. *J. Neurosci.* 41:5157.

Gavello, D., Calorio, C., Franchino, C., Cesano, F., Carabelli, V., Carbone, E., et al. (2018). Early alterations of hippocampal neuronal firing induced by Abeta42. *Cereb. Cortex* 28, 433–446. doi: 10.1093/cercor/bhw377

Gilbert, J., Shu, S., Yang, X., Lu, Y., Zhu, L.-Q., and Man, H.-Y. (2016). β-Amyloid triggers aberrant over-scaling of homeostatic synaptic plasticity. *Acta Neuropathol. Commun.* 4:131.

Handler, M., Yang, X., and Shen, J. (2000). Presenilin-1 regulates neuronal differentiation during neurogenesis. *Development* 127, 2593–2606.

Hatami, A., Albay, R. III, Monjazeb, S., Milton, S., and Glabe, C. (2014). Monoclonal antibodies against Aβ42 fibrils distinguish multiple aggregation state polymorphisms *in vitro* and in Alzheimer disease brain. *J. Biol. Chem.* 289, 32131–32143. doi: 10.1074/jbc.M114.594846

Heath, M. J., Womack, M. D., and Macdermott, A. B. (1994). Substance P elevates intracellular calcium in both neurons and glial cells from the dorsal horn of the spinal cord. *J. Neurophysiol.* 72, 1192–1198. doi: 10.1152/jn.1994.72.3.1192

Hedstrom, K. L., Ogawa, Y., and Rasband, M. N. (2008). AnkyrinG is required for maintenance of the axon initial segment and neuronal polarity. *J. Cell Biol.* 183, 635–640.

Hollnagel, J. O., Elzoheiry, S., Gorgas, K., Kins, S., Beretta, C. A., Kirsch, J., et al. (2019). Early alterations in hippocampal perisomatic GABAergic synapses and network oscillations in a mouse model of Alzheimer's disease amyloidosis. *PLoS One* 14:e0209228. doi: 10.1371/journal.pone.0209228

Iwata, N., Mizukami, H., Shirotani, K., Takaki, Y., Muramatsu, S.-I., Lu, B., et al. (2004). Presynaptic localization of neprilysin contributes to efficient clearance of amyloid-β peptide in mouse brain. *J. Neurosci.* 24, 991–998. doi: 10.1523/JNEUROSCI.4792-03.2004

Jamann, N., Dannehl, D., Lehmann, N., Wagener, R., Thielemann, C., Schultz, C., et al. (2021). Sensory input drives rapid homeostatic scaling of the axon initial segment in mouse barrel cortex. *Nat. Commun.* 12:23. doi: 10.1038/s41467-020-20232-x

Kagan, B. L., Hirakura, Y., Azimov, R., Azimova, R., and Lin, M. C. (2002). The channel hypothesis of Alzheimer's disease: current status. *Peptides* 23, 1311–1315. doi: 10.1016/s0196-9781(02)00067-0

Kamenetz, F., Tomita, T., Hsieh, H., Seabrook, G., Borchelt, D., Iwatsubo, T., et al. (2003). APP processing and synaptic function. *Neuron* 37, 925–937.

Kang, J. E., Lim, M. M., Bateman, R. J., Lee, J. J., Smyth, L. P., Cirrito, J. R., et al. (2009). Amyloid-beta dynamics are regulated by orexin and the sleep-wake cycle. *Science* 326, 1005–1007. doi: 10.1126/science.1180962

Kashyap, G., Bapat, D., Das, D., Gowaikar, R., Amritkar, R. E., Rangarajan, G., et al. (2019). Synapse loss and progress of Alzheimer's disease –A network model. *Sci. Rep.* 9:6555.

Kawahara, M., and Kuroda, Y. (2000). Molecular mechanism of neurodegeneration induced by Alzheimer's beta-amyloid protein: channel formation and disruption of calcium homeostasis. *Brain Res. Bull.* 53, 389–397.

Koo, E. H., Sisodia, S. S., Archer, D. R., Martin, L. J., Weidemann, A., Beyrreuther, K., et al. (1990). Precursor of amyloid protein in Alzheimer disease undergoes fast anterograde axonal transport. *Proc. Natl. Acad. Sci. U.S.A.* 87, 1561–1565.

Kuchibhotla, K. V., Goldman, S. T., Lattarulo, C. R., Wu, H. Y., Hyman, B. T., and Bacskai, B. J. (2008). Abeta plaques lead to aberrant regulation of calcium homeostasis *in vivo* resulting in structural and functional disruption of neuronal networks. *Neuron* 59, 214–225. doi: 10.1016/j.neuron.2008.06.008

Lacor, P. N., Buniel, M. C., Chang, L., Fernandez, S. J., Gong, Y., Viola, K. L., et al. (2004). Synaptic targeting by Alzheimer's-related amyloid beta oligomers. *J. Neurosci.* 24, 10191–10200.

Lauren, J., Gimbel, D. A., Nygaard, H. B., Gilbert, J. W., and Strittmatter, S. M. (2009). Cellular prion protein mediates impairment of synaptic plasticity by amyloid-beta oligomers. *Nature* 457, 1128–1132.

Lee, S. H., Kang, J., Ho, A., Watanabe, H., Bolshakov, V. Y., and Shen, J. (2020). APP family regulates neuronal excitability and synaptic plasticity but not neuronal survival. *Neuron* 108, 676.e8–690.e8.

Lerdkrai, C., Asavapanumas, N., Brawek, B., Kovalchuk, Y., Mojtahedi, N., Olmedillas del Moral, M., et al. (2018). Intracellular Ca(2+) stores control *in vivo* neuronal hyperactivity in a mouse model of Alzheimer's disease. *Proc. Natl. Acad. Sci. U.S.A.* 115, E1279–E1288. doi: 10.1073/pnas.1714409115

Martinsson, I., Capetillo-Zarate, E., Faideau, M., Willen, K., Esteras, N., Frykman, S., et al. (2019). APP depletion alters selective pre- and post-synaptic proteins. *Mol. Cell Neurosci.* 95, 86–95. doi: 10.1016/j.mcn.2019.02.003

Mata, G., Cuesto, G., Heras, J., Morales, M., Romero, A., and Rubio, J. (2017). "SynapCountJ: a validated tool for analyzing synaptic densities in neurons," in *Biomedical Engineering Systems and Technologies*, eds A. Fred and H. Gamboa (Cham: Springer International Publishing), 41–55. doi: 10.1002/jnr.23353

Minkeviciene, R., Rheims, S., Dobszay, M. B., Zilberter, M., Hartikainen, J., Fülöp, L., et al. (2009). Amyloid beta-induced neuronal hyperexcitability triggers progressive epilepsy. *J. Neurosci.* 29, 3453–3462. doi: 10.1523/JNEUROSCI.5215-08.2009

Nimmrich, V., Grimm, C., Draguhn, A., Barghorn, S., Lehmann, A., Schoemaker, H., et al. (2008). Amyloid beta oligomers (A beta(1-42) globulomer) suppress spontaneous synaptic activity by inhibition of P/Q-type calcium currents. *J. Neurosci.* 28, 788–797. doi: 10.1523/JNEUROSCI.4771-07.2008

Pandis, D., and Scarmeas, N. (2012). Seizures in Alzheimer disease: clinical and epidemiological data. *Epilepsy Curr.* 12, 184–187.

Perdigão, C., Barata, M. A., Araújo, M. N., Mirfakhar, F. S., Castanheira, J., and Guimas Almeida, C. (2020). Intracellular trafficking mechanisms of synaptic dysfunction in Alzheimer's disease. *Front. Cell Neurosci.* 14:72. doi: 10.3389/fncel.2020.00072

Puzzo, D., Privitera, L., Leznik, E., Fa, M., Staniszewski, A., Palmeri, A., et al. (2008). Picomolar amyloid-beta positively modulates synaptic plasticity and memory in hippocampus. *J. Neurosci.* 28, 14537–14545. doi: 10.1523/JNEUROSCI.2692-08.2008

Quintino, L., Manfre, G., Wettergren, E. E., Namislo, A., Isaksson, C., and Lundberg, C. (2013). Functional neuroprotection and efficient regulation of GDNF using destabilizing domains in a rodent model of Parkinson's disease. *Mol. Ther.* 21, 2169–2180. doi: 10.1038/mt.2013.169

Rama, N., Goldschneider, D., Corset, V., Lambert, J., Pays, L., and Mehlen, P. (2012). Amyloid precursor protein regulates netrin-1-mediated commissural axon outgrowth. *J. Biol. Chem.* 287, 30014–30023. doi: 10.1074/jbc.M111.324780

Reyes-Marin, K. E., and Nuñez, A. (2017). Seizure susceptibility in the APP/PS1 mouse model of Alzheimer's disease and relationship with amyloid β plaques. *Brain Res.* 1677, 93–100.

Roos, T. T., Garcia, M. G., Martinsson, I., Mabrouk, R., Israelsson, B., Deierborg, T., et al. (2021). Neuronal spreading and plaque induction of intracellular Aβ and its disruption of Aβ homeostasis. *Acta Neuropathol.* 142, 669–687.

Sadigh-Eteghad, S., Talebi, M., Farhoudi, M., Golzari, S. E. J., Sabermarouf, B., and Mahmoudi, J. (2014). Beta-amyloid exhibits antagonistic effects on alpha 7 nicotinic acetylcholine receptors in orchestrated manner. *J. Med. Hypothes. Ideas* 8, 49–52.

Sadleir, K. R., Kandalepas, P. C., Buggia-Prévot, V., Nicholson, D. A., Thinakaran, G., and Vassar, R. (2016). Presynaptic dystrophic neurites surrounding amyloid

plaques are sites of microtubule disruption, BACE1 elevation, and increased Aβ generation in Alzheimer's disease. *Acta Neuropathol.* 132, 235–256. doi: 10.1007/s00401-016-1558-9

Scharfman, H. E. (2012). Alzheimer's disease and epilepsy: insight from animal models. *Future Neurol.* 7, 177–192.

Siskova, Z., Justus, D., Kaneko, H., Friedrichs, D., Henneberg, N., Beutel, T., et al. (2014). Dendritic structural degeneration is functionally linked to cellular hyperexcitability in a mouse model of Alzheimer's disease. *Neuron* 84, 1023–1033. doi: 10.1016/j.neuron.2014.10.024

Slomowitz, E., Styr, B., Vertkin, I., Milshtein-parush, H., Nelken, I., Slutsky, M., et al. (2015). Interplay between population firing stability and single neuron dynamics in hippocampal networks. *eLife* 4:e04378. doi: 10.7554/eLife.04378

Stranahan, A. M., and Mattson, M. P. (2010). Selective vulnerability of neurons in layer II of the entorhinal cortex during aging and Alzheimer's disease. *Neural Plast.* 2010:108190.

Takahashi, R. H., Almeida, C. G., Kearney, P. F., Yu, F., Lin, M. T., Milner, T. A., et al. (2004). Oligomerization of Alzheimer's beta-amyloid within processes and synapses of cultured neurons and brain. *J. Neurosci.* 24, 3592–3599.

Takahashi, R. H., Milner, T. A., Li, F., Nam, E. E., Edgar, M. A., Yamaguchi, H., et al. (2002). Intraneuronal Alzheimer abeta42 accumulates in multivesicular bodies and is associated with synaptic pathology. *Am. J. Pathol.* 161, 1869–1879.

Tampellini, D., Capetillo-Zarate, E., Dumont, M., Huang, Z., Yu, F., Lin, M. T., et al. (2010). Effects of synaptic modulation on beta-amyloid, synaptophysin, and memory performance in Alzheimer's disease transgenic mice. *J. Neurosci.* 30, 14299–14304.

Tampellini, D., Rahman, N., Gallo, E. F., Huang, Z., Dumont, M., Capetillo-Zarate, E., et al. (2009). Synaptic activity reduces intraneuronal Abeta, promotes APP transport to synapses, and protects against Abeta-related synaptic alterations. *J. Neurosci.* 29, 9704–9713. doi: 10.1523/JNEUROSCI.2292-09.2009

Texidó, L., Martín-Satué, M., Alberdi, E., Solsona, C., and Matute, C. (2011). Amyloid β peptide oligomers directly activate NMDA receptors. *Cell Calcium* 49, 184–190. doi: 10.1016/j.ceca.2011.02.001

Thiagarajan, T. C., Piedras-Renteria, E. S., and Tsien, R. W. (2002). alpha- and betaCaMKII. Inverse regulation by neuronal activity and opposing effects on synaptic strength. *Neuron* 36, 1103–1114. doi: 10.1016/s0896-6273(02)01049-8

Turrigiano, G. (2012). Homeostatic synaptic plasticity: local and global mechanisms for stabilizing neuronal function. *Cold Spring Harb. Perspect. Biol.* 4:a005736.

Turrigiano, G. G. (2008). The self-tuning neuron: synaptic scaling of excitatory synapses. *Cell* 135, 422–435. doi: 10.1016/j.cell.2008.10.008

Turrigiano, G. G., Leslie, K. R., Desai, N. S., Rutherford, L. C., and Nelson, S. B. (1998). Activity-dependent scaling of quantal amplitude in neocortical neurons. *Nature* 391, 892–896.

Vargas, L. M., Cerpa, W., Munoz, F. J., Zanlungo, S., and Alvarez, A. R. (2018). Amyloid-beta oligomers synaptotoxicity: the emerging role of EphA4/c-Abl signaling in Alzheimer's disease. *Biochim. Biophys. Acta Mol. Basis Dis.* 1864, 1148–1159. doi: 10.1016/j.bbadis.2018.01.023

Vossel, K. A., Beagle, A. J., Rabinovici, G. D., Shu, H., Lee, S. E., Naasan, G., et al. (2013). Seizures and epileptiform activity in the early stages of Alzheimer disease. *JAMA Neurol.* 70, 1158–1166.

Wefelmeyer, W., Puhl, C. J., and Burrone, J. (2016). Homeostatic plasticity of subcellular neuronal structures: from inputs to outputs. *Trends Neurosci.* 39, 656–667. doi: 10.1016/j.tins.2016.08.004

Westmark, C. J., and Malter, J. S. (2007). FMRP mediates mGluR5-dependent translation of amyloid precursor protein. *PLoS Biol.* 5:e0050052. doi: 10.1371/journal.pbio.0050052

Willén, K., Edgar, J. R., Hasegawa, T., Tanaka, N., Futter, C. E., and Gouras, G. K. (2017). Aβ accumulation causes MVB enlargement and is modelled by dominant negative VPS4A. *Mol. Neurodegener.* 12:61. doi: 10.1186/s13024-017-0203-y

Willen, K., Sroka, A., Takahashi, R. H., and Gouras, G. K. (2017). Heterogeneous association of alzheimer's disease-linked amyloid-beta and amyloid-beta protein precursor with synapses. *J. Alzheimers. Dis.* 60, 511–524. doi: 10.3233/JAD-170262

Yang, L., Wang, Z., Wang, B., Justice, N. J., and Zheng, H. (2009). Amyloid precursor protein regulates Cav1.2 L-type calcium channel levels and function to influence GABAergic short-term plasticity. *J. Neurosci.* 29, 15660–15668. doi: 10.1523/JNEUROSCI.4104-09.2009

Zarhin, D., Atsmon, R., Ruggiero, A., Baeloha, H., Shoob, S., Scharf, O., et al. (2022). Disrupted neural correlates of anesthesia and sleep reveal early circuit dysfunctions in Alzheimer models. *Cell Rep.* 38:110268. doi: 10.1016/j.celrep.2021.110268

Zott, B., Simon, M. M., Hong, W., Unger, F., Chen-Engerer, H. J., Frosch, M. P., et al. (2019). A vicious cycle of β amyloid-dependent neuronal hyperactivation. *Science* 365, 559–565. doi: 10.1126/science.aay0198

Conflict of Interest: The authors declare that the research was conducted in the absence of any commercial or financial relationships that could be construed as a potential conflict of interest.

Publisher's Note: All claims expressed in this article are solely those of the authors and do not necessarily represent those of their affiliated organizations, or those of the publisher, the editors and the reviewers. Any product that may be evaluated in this article, or claim that may be made by its manufacturer, is not guaranteed or endorsed by the publisher.